Note

Fast calculation of the tokamak vertical instability

K.E.J. Olofsson[1]

[1] General Atomics, P.O. Box 85608, San Diego, CA 92186-5608, USA

E-mail: olofsson@fusion.gat.com
19 April 2022

Abstract. There has been recent interest in fast calculations of the tokamak axisymmetric vertical instability for real time feedback control purposes. It is shown that the maximum eigenvalue for the basic rigid version of this stability problem can be obtained by finding the positive root to a simple scalar function. This function can be generalized to include plasma mass and has complexity linear in the number of conductive elements. The formulation is based on standard matrix decompositions of the fixed-geometry part of the eigenproblem. The calculation bottleneck is the summary of mutual inductances from the reconstructed equilibrium current density. The with-mass spectrum can be made fully real-valued by the addition of a critical amount of damping with negligible effect on the vertical growth rate. The calculation has been implemented in the plasma control system at the DIII-D tokamak and used in experiments.

Keywords: Tokamak, stability, control

Submitted to: *Plasma Phys. Control. Fusion*

1. Introduction

The vertical instability of elongated toroidal plasmas constitute a basic constraint in the design and operation of tokamak experiments [1–4]. It is routinely stabilized using feedback control with poloidal field coils. Recent experimental work with the aim to increase the operational reliability of tokamaks has incorporated real time calculation and estimation of the vertical growth rate [5–8]. The idea is to (dynamically) detect the proximity to parameter regime boundaries where the vertical feedback circuit can no longer maintain stability in the presence of perturbations. Ignoring such boundaries can otherwise lead to disruptions through so called vertical displacement events, which may damage the tokamak itself [9, 10].

This note provides two specific contributions. First, a new lightweight numerical calculation of the basic version of the rigid-motion vertical eigenvalue problem is reported. It is based on pre-calculating a sequence of two matrix coordinate transformations; a well-known simultaneous diagonalization of two quadratic forms of which one is positive definite [11, 12]. Its implementation was instrumental in recent

experimental work at the DIII-D tokamak [7] and is less complex and about an order of magnitude faster than that reported in [5] albeit at some loss of generality. Second, it is shown that the same coordinate transformations render the with-mass version of the rigid vertical stability problem equally simple. A closed-form approximate critical value for an effective damping parameter is provided for the with-mass version of the eigenproblem. This damping removes the rigid $n = 0$ "Alfvénic" oscillation, with very small impact on the vertical growth rate.

The remainder of this note is organized as follows. Section 2 describes the basic engineering physics model, derives the coordinate transformations, and presents the main results. Section 3 outlines the implementation, details the specific DIII-D instance of the eigenproblem, and compares it to a standard rigid code. Numerical results are shown for a DIII-D plasma to gauge the impact of the added damping. All these calculations are done with the DIII-D standard engineering physics geometry. This note concludes with a short discussion in section 4.

2. Calculation

For the purposes here it suffices to include only one mechanical degree of freedom (rigid vertical displacement z). A compact self-contained preparation of the relevant equations for plasma vertical motion is obtained by writing an appropriate magneto-mechanical [13] Lagrangian

$$\mathcal{L} = \frac{1}{2} m\dot{z}^2 + \frac{1}{2}\bar{\mathbf{I}}^T \bar{M}(z)\bar{\mathbf{I}} + \phi \tag{1}$$

which has as many electrical degrees of freedom as there are conducting axisymmetric elements. The first term in (1) holds the mechanical kinetic energy, the second term corresponds to magnetostatic energy for the configuration, and the third term is a electrostatic potential ϕ (used to book-keep the applied voltage). Keeping in mind that a current is a momentum variable in the Lagrangian, the Euler-Lagrange equations encoded by (1) yield

$$\frac{\mathrm{d}}{\mathrm{dt}}\left(m\dot{z}\right) - \frac{1}{2}\sum_{i,j}\frac{\partial \bar{M}_{i,j}(z)}{\partial z}\bar{I}_i\bar{I}_j = -\nu\dot{z} \tag{2}$$

$$\frac{\mathrm{d}}{\mathrm{dt}}\left(\bar{M}(z)\bar{\mathbf{I}}\right) - \bar{\mathbf{V}} = -\bar{R}\bar{\mathbf{I}} \tag{3}$$

when augmented with Rayleigh dissipation terms $\mathcal{R} = (1/2)\nu\dot{z}^2 + (1/2)\bar{\mathbf{I}}^T\bar{R}\bar{\mathbf{I}}$ [13, 14]. Coupled nonlinear equations (2)-(3) describe the vertical momentum and mutually inductive circuit respectively. $\bar{R}$ is a diagonal matrix with conductor resistances on the diagonal, $\bar{I}_i$ are the current elements in $\bar{\mathbf{I}}$, and $\bar{\mathbf{V}}$ is a vector of applied voltages. The total plasma current I_p is included as one of the elements in vector $\bar{\mathbf{I}}$, the other elements correspond to poloidal field coils and passive vessel elements. In this lumped formulation, only the elements associated with I_p in the matrix $\bar{M}(z)$ depend on z. The plasma self-inductance $\bar{M}_{p,p}$ is actually a constant independent of z, but all the other elements $\bar{M}_{i,p} = \bar{M}_{p,i}$, $i \neq p$, are functions of z.

When I_p and the plasma mass m are treated as constants, the linearized dynamical system

$$m\ddot{z} + \nu\dot{z} \quad = Kz + \mathbf{b}^T\mathbf{x} \tag{4}$$

$$M\dot{\mathbf{x}} + R\mathbf{x} = \ -\mathbf{b}\dot{z} \tag{5}$$

can be obtained from (2)-(3) above. Equations (4)-(5) introduces

$$K = I_p\mathbf{I}_0^T\frac{\partial\mathbf{g}}{\partial z} \tag{6}$$

and

$$\mathbf{b} = I_p\mathbf{g} \tag{7}$$

where

$$\mathbf{g} = \left[\frac{\partial M_{1,p}}{\partial z}, \frac{\partial M_{2,p}}{\partial z}, \ldots, \frac{\partial M_{J,p}}{\partial z}\right]^T \tag{8}$$

collects gradients of mutual inductances $M_{j,p}$ between the plasma and the J fixed conductors $j = 1 \ldots J$, and $\mathbf{I}_0$ is the vector of currents in the same J fixed conductors. The elements $M_{j,p}$ are the same as the entries in the column of $\bar{M}$ in eq. (3), but omitting the self-inductance $\bar{M}_{p,p}$ which is never needed here. The matrix M is formed from $\bar{M}$ by deleting its row and column corresponding to the plasma current state. Similarly, the plasma resistance $\bar{R}_{p,p}$ drops out of this fixed-I_p model.

The state $\mathbf{x}$ in (4)-(5) now holds the perturbed currents, $\mathbf{I} - \mathbf{I}_0 = \mathbf{x}$. The key observation is that only the scalar K (dimension N/m) and the vector $\mathbf{b}$ (dimension Wb/m) depend on the specific plasma equilibrium. M only stores mutual inductances between fixed-position conductors, and (the diagonal of) R only holds nominally constant resistances for the same fixed conductors (active and passive). The standard (massless) condition for vertical instability is geometrical (not involving data in R) and is here represented by $\mathbf{b}^T M^{-1}\mathbf{b} > K > 0$ [3].

2.1. Simultaneous diagonalization

The application of two types of standard matrix decompositions renders (5) diagonal. First, M is symmetric positive definite so it has a Cholesky factorization

$$M = LL^T \tag{9}$$

where L is lower triangular. Second, whenever $R = R^T$ (which specifically holds here since R is diagonal), the real-valued symmetric eigenvalue decomposition

$$L^{-1}RL^{-T} = Q = U\Lambda U^T \tag{10}$$

can be used on the intermediate matrix $Q = Q^T$ formed using L as a symmetric weighting on R. In (10), U is orthonormal and Λ is diagonal with non-negative elements $\lambda_i \geq 0$. In the new coordinate

$$\boldsymbol{\xi} = U^T L^T\mathbf{x} \tag{11}$$

system (5) becomes diagonalized

$$\dot{\boldsymbol{\xi}} = -\Lambda\boldsymbol{\xi} - \boldsymbol{\beta}\dot{z} \tag{12}$$

where

$$\boldsymbol{\beta} = U^T L^{-1}\mathbf{b} \tag{13}$$

which is a triangular backsubstitution followed by a orthonormal transformation. It holds $\sum_i \xi_i^2 = \mathbf{x}^T M\mathbf{x}$, $\sum_i \beta_i^2 = \mathbf{b}^T M^{-1}\mathbf{b}$, and $\boldsymbol{\beta}^T\boldsymbol{\xi} = \mathbf{b}^T\mathbf{x}$.

2.2. Standard massless case

Neglecting both plasma mass m and damping parameter ν results in the force balance condition $Kz + \mathbf{b}^T\mathbf{x} = 0$ replacing equation (4). Combining the time-derivative of this rank-1 constraint with (5) results in $\left(M - K^{-1}\mathbf{b}\mathbf{b}^T\right)\dot{\mathbf{x}} + R\mathbf{x} = \mathbf{0}$. Now using (11) results in $\left(I - K^{-1}\boldsymbol{\beta}\boldsymbol{\beta}^T\right)\dot{\boldsymbol{\xi}} + \Lambda\boldsymbol{\xi} = \mathbf{0}$. Finally, by applying the Sherman-Morrison formula and introducing the square root coordinate $\boldsymbol{\chi} = \Lambda^{1/2}\boldsymbol{\xi}$, this becomes an eigenvalue problem for a symmetric rank-1 update of a diagonal matrix

$$A_1 = -\Lambda + \alpha \times \mathbf{c}\mathbf{c}^T \tag{14}$$

in the sense, $\dot{\boldsymbol{\chi}} = A_1\boldsymbol{\chi}$, where $\mathbf{c} = \Lambda^{1/2}\boldsymbol{\beta}$ and $\alpha = -\left(K - \boldsymbol{\beta}^T\boldsymbol{\beta}\right)^{-1} > 0$. From the matrix literature [15] it follows that the maximum eigenvalue calculation for (14) is reduced to finding the root $\lambda > 0$ to the equation

$$0 = 1 - \frac{\lambda}{K}\sum_i \frac{\beta_i^2}{\lambda_i + \lambda} \tag{15}$$

where an upper bound (not very tight) is $\bar{\lambda} = \max_i(-\lambda_i) + \alpha\sum_i \beta_i^2\lambda_i$. Solving (15) in using bisection with initial bracket $\left[0, \bar{\lambda}\right]$ will always work whenever the root exists (i.e. assuming $K - \sum_i \beta_i^2 < 0$, $K > 0$).

2.3. Inductive stability margin

In the context of this rigid model, it is also possible to solve a similar scalar equation for the inductive stability margin m_s, introduced in [3], associated with the vertical displacement. This quantity is independent of the conductor resistivities and can be equated with the positive root $x > 0$ of

$$0 = 1 - \frac{1}{K}\sum_i \frac{\tilde{b}_i^2}{1 + x} \tag{16}$$

with the upper bound $\bar{x} = -1 + \tilde{\mathbf{b}}^T\tilde{\mathbf{b}}/K$, and where the vector $\tilde{\mathbf{b}} = L^{-1}\mathbf{b}$ was introduced. The amount of work required to prepare data for the calculation of m_s is less than the work required for λ since matrix U is not used. This has to be the case since the resistor data in R cannot influence this quantity.

2.4. Generalized with-mass case

With the "balanced" change of coordinates $\boldsymbol{\zeta} = \left[\sqrt{K}z, \sqrt{m}\dot{z}, \mathbf{x}^T LU\right]^T$ the total system matrix for (4)-(5) becomes

$$A = \begin{pmatrix} 0 & \sqrt{K/m} & \mathbf{0}^T \\ \sqrt{K/m} & -\nu/m & \boldsymbol{\beta}^T/\sqrt{m} \\ \mathbf{0} & -\boldsymbol{\beta}/\sqrt{m} & -\Lambda \end{pmatrix} \tag{17}$$

in the sense $\dot{\boldsymbol{\zeta}} = A\boldsymbol{\zeta}$, and it can be shown (Schur complements and the matrix determinant lemma) that the equation for its maximum eigenvalue

$$0 = 1 - \frac{\lambda}{K}\left(\nu + \sum_i \frac{\beta_i^2}{\lambda_i + \lambda}\right) - \frac{m}{K}\lambda^2 \tag{18}$$

is a generalization of (15). Equation (18) is also valid for $m = 0$, $\nu > 0$ (massless but damped).

2.5. Critical dissipation

The introduction of a small mass here creates a (fragile) damped oscillatory "plasma" mode [16]. This mode is typically ignored, since it corresponds to an unrealistically rapid oscillation settling at the force balance condition. An approximation of this mode is found by solving

$$\lambda^2 + \lambda\frac{\nu}{m} - K/m + \frac{1}{m}\sum_i \beta_i^2 = 0 \tag{19}$$

assuming it has a complex-conjugate pair solution with comparatively large $|\lambda|$: $\lambda_i/|\lambda|$ small. The solution to (19) is complex valued with $\mathrm{Re}\lambda = -\nu/(2m)$ and $\mathrm{Im}\lambda = \pm\sqrt{4\omega_0^2 - \nu^2/m^2}/2$ whenever

$$\nu < \nu_{crit} = 2m\omega_0 \tag{20}$$

with the (undamped) angular frequency

$$\omega_0 = \sqrt{\frac{\sum_i \beta_i^2 - K}{m}} \tag{21}$$

As $m \to 0$ the solution modulus $|\lambda|$ will be large. By setting the effective damping parameter roughly at or above ν_{crit}, one might expect the spectrum of (17) to be non-complex. Below, it is demonstrated that this critical damping has insignificant impact on the vertical growth rate using DIII-D parameters.

3. Numerical applications

3.1. Scaling of solver performance

The work required to solve for the eigenvalues is determined by the number of conducting elements J. The number of numerical operations for a generic case is $\sim J^3$. The front-loaded simultaneous diagonalization ($\sim J^3$) takes this down to $\sim J$ assuming a constant

number of bisections, but at the remaining runtime cost of a preparatory $\sim J^2$ vector transformation. The significance of this reduction in complexity can be shown clearly with the execution time scaling in Figure 1.

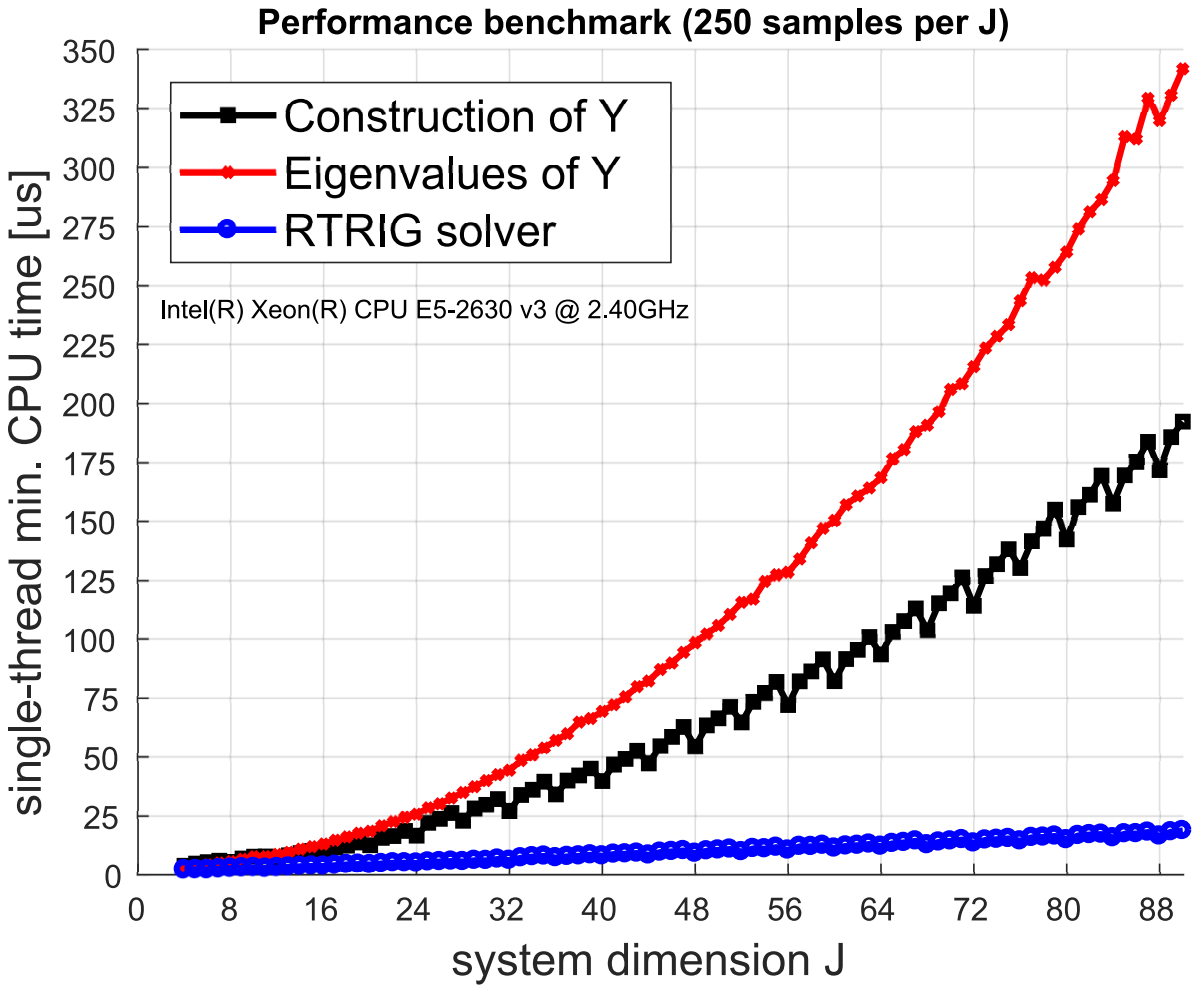

Figure 1. Scaling of execution time, comparing the RTRIG solver (this Note) versus a standard approach of building a symmetrized matrix Y (22) and computing only its eigenvalues (no eigenvectors, which would be much slower). Since this benchmark ran on a non-real-time operating system, the minimum execution time across 250 trials is reported. The exact wall-clock numbers depend on CPU model, clock-speed, numerical libraries, and possibly compiler options. The scaling with J does not depend on those details.

Assuming that (7) and (6) are available, the standard massless eigenproblem is that of finding the eigenvalues of

$$Y = -R^{1/2}\left(M - \frac{1}{K}\mathbf{b}\mathbf{b}^T\right)^{-1} R^{1/2} \tag{22}$$

where (in this benchmark) it is assumed that R is diagonal with non-negative elements ($R^{1/2}$ holds the square root of the diagonal). For each dimension J, a unique problem instance is generated such that M is a random symmetric positive definite matrix,

$\mathbf{b}$ is a vector of standard normal variates, $K = \eta \mathbf{b}^T M^{-1} \mathbf{b}$, where $0 < \eta < 1$ is a uniform random number, and R has unformly random diagonal elements (independently drawn the same way as η). The run-time cost using single-threaded double-precision numerical linear algebra is then measured (repeatedly for each J with regenerated problem instances). The run-time cost for the standard solution is composed of two parts: the construction of Y, and the computation of the eigenvalues of Y. The sum of these two execution times (black and red traces respectively) should be compared to the RTRIG approach (shown as the blue trace). The RTRIG run-time cost is the sum of computing (13) and bisecting (15).

For DIII-D, the total number of conductors is 20 (active) + 28 (passive). So the length of vector (8) is $J = 48$. In [5], a system model with size $J = 79$ is reported. Figure 1 demonstrates $\sim 10\times$ (and larger) reductions in execution times using RTRIG for both of these two cases. Notice that this benchmark only compares the vertical-stability-specific part of the calculation. There is additional significant run-time cost in processing the reconstructed equilibrium to get (8) and (6). If the RTRIG solver is used, these other more generic calculations become the bottleneck.

3.2. Experimental deployment

A program that solves (15) was implemented in the DIII-D plasma control system (PCS) [17]. The implementation is single-threaded and constitute a self-contained task that post-processes the real-time magnetics-only equilibrium reconstructions (EFITs) [18] which the PCS generates (roughly) once per millisecond. The total calculation requires $\sim 200\,\mu$sec (using present PCS hardware), of which nearly all time is spent preparing the vector (7) and scalar (6); according to Figure 1 it is estimated that only $\sim 10\,\mu$sec is spent on the actual solve. The calculation of the mutuals' gradients required for (8) and (6) is done using finite differencing (three-point stencil) and inner products repeatedly involving the entire 65×65 EFIT grid toroidal current distribution (which also need to be extracted from the EFIT). Weight vectors for this are pre-computed as part of EFIT itself, and consists of mutual inductances between each conductor and the 4225 plasma grid cells. The eigenproblem is linearized around the presumed situation where the passive element currents are set to zero.

Figure 2 shows an example comparison of the standard code RZRIG (which is a rigid massless code but which also includes a radial degree of freedom) [9] evaluated on standard offline EFITs, with RTRIG as evaluated on real time EFITs (which are not as accurate). The difference between RZRIG and RTRIG both evaluated on the same offline EFITs is not visible on the scale of this plot. Those differences (and more) are instead tabulated, for a set of time-slices, in Table 1.

The experiment shown in Figure 2 is a lower-single-null plasma where a pre-programmed ramp in (upper) plasma elongation is started at $t = 2.1\,$sec. As the elongation is increased (while keeping the magnetic null at a constant position) the plasma becomes increasingly vertically unstable. The end of the pre-programmed ramp

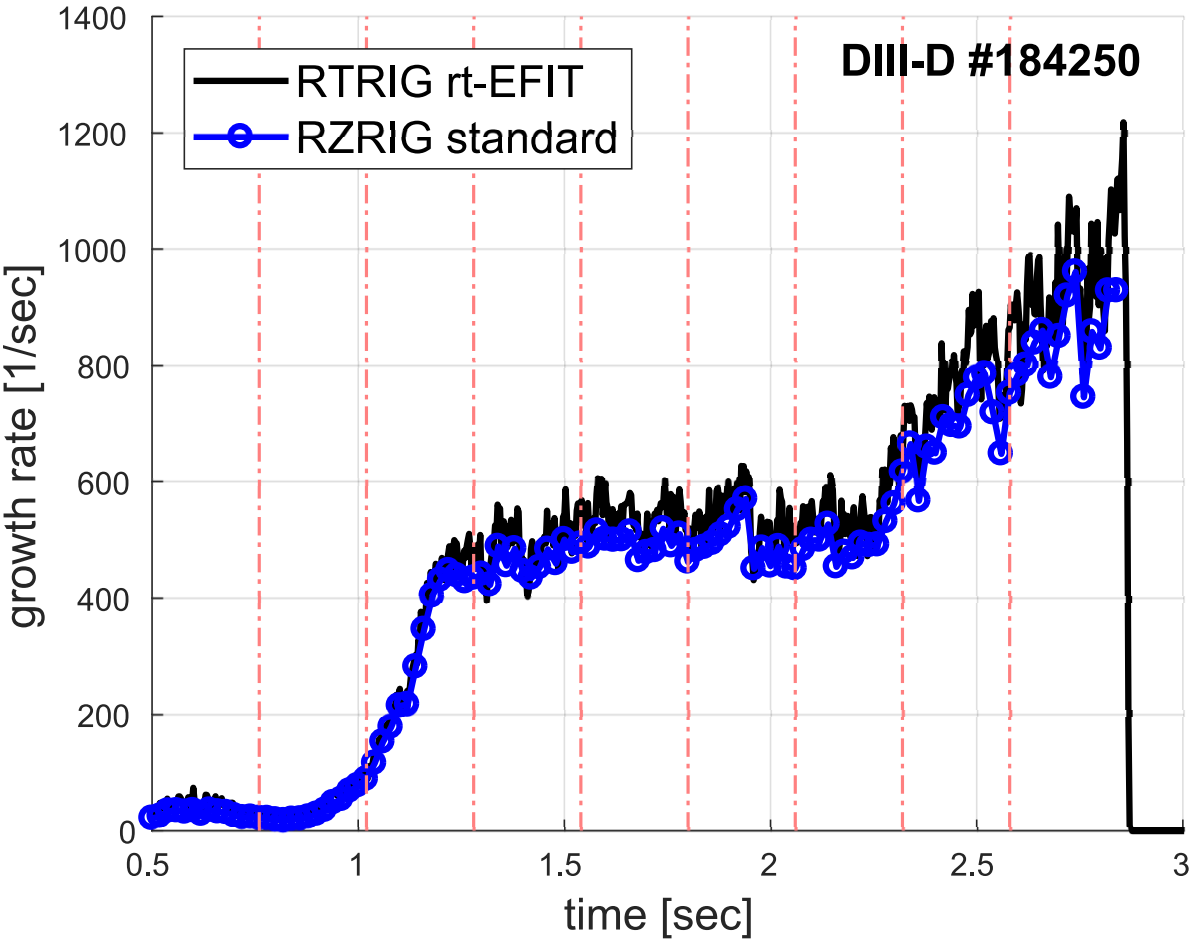

Figure 2. Comparison of RZRIG (standard code) evaluated on standard offline magnetics-only equilibrium reconstructions, and RTRIG (this note) as evaluated online based on streaming real-time magnetics-only equilibrium reconstructions. The vertical dash-dotted lines mark specific time-slices where more detailed comparisons are made between various versions of the eigenproblem (Table 1).

is at $t = 3.0\,\text{sec}$ but is never reached since the plasma disrupts as a result of the induced vertical displacement event. DIII-D plasmas, as in Figure 2, experience loss of vertical stability control as the growth rate $(dz/dt)/z$ approaches and exceeds $\sim 1000\,\text{sec}^{-1}$. In this particular shot RTRIG ran in real time "passively", meaning that no action was taken based off of the value of λ calculated online. RTRIG has also been used in "active" (feedback based on λ) mode [7] and replaces the previous RZRIG emulation [8].

3.3. Example tabulation of λ, ν_{crit}, and ω_0

Denote the growth rate solution to (17) by $\lambda(m, \nu)$, so that $\lambda(0, 0)$ is equal to the standard non-damped massless solution, $\lambda(m, 0)$ is the with-mass non-damped solution, and $\lambda(m, \nu_*)$ is the critically damped with-mass solution. Table 1 shows values of $\lambda(\cdot, \cdot)$ for specific time slices marked by dash-dotted lines in Figure 2. Realistic mass-values for DIII-D plasmas are in the milligram range. In the table, $m = 5.0 \times 10^{-6}\,\text{kg}$ is used. The

Table 1. Comparison of different variants $\lambda(m,\nu)$ of the vertical growth rate for the subset of magnetics-only standard EFIT time slices marked in Figure 2. Also comparison of the accuracy of the critical ν approximation. The plasma mass is set to $m = 5.0\,\mathrm{mg}$. The RTRIG column corresponds to $\lambda(0,0)$, and $f_0 = (2\pi)^{-1}\omega_0$.

time [s]	RZRIG [s^{-1}]	RTRIG	$\lambda(m,0)$	$\lambda(m,\nu_*)$	ν_* [Ns/m]	ν_{crit}	f_0 [kHz]
0.760	20.9588	20.912	20.912	20.8808	2.6007	2.5967	41.328
1.020	88.2864	87.9845	87.9844	87.623	2.8168	2.8119	44.754
1.280	434.023	433.093	433.089	428.798	2.3010	2.2937	36.505
1.540	492.719	491.638	491.632	486.401	2.2723	2.2646	36.043
1.800	461.862	460.724	460.719	456.075	2.3045	2.2971	36.560
2.060	450.42	449.313	449.309	444.909	2.3311	2.3238	36.985
2.320	616.362	615.541	615.53	607.782	2.1654	2.1570	34.329
2.580	752.247	751.657	751.637	740.588	2.0752	2.0659	32.880

expected ordering of growth-rates is: $\lambda(0,0) > \lambda(m,0) > \lambda(m,\nu_*)$, with the additional inequality RZRIG $> \lambda(0,0)$, since RZRIG has an additional degree of freedom. The difference between RTRIG, $\lambda(0,0)$, and its with-mass perturbation $\lambda(m,0)$ is around the fifth digit for this mass value. The critical value of the damping parameter ν_* is found by numerically bisecting the location where matrix (17) switches from all-real to a complex spectrum. The relative difference between ν_* and the approximation (20) is $\sim 10^{-2}$ for this mass. The relative difference between ω_0, approximation (21), and actual ω_* (oscillatory with-mass undamped mode) is $\sim 10^{-5}$. These differences vanish as m goes to zero.

4. Discussion

In this Note, a fast new calculation of the rigid displacement vertical stability of a tokamak plasma was presented. The method was implemented on the DIII-D tokamak. The new solver formulation dramatically outperforms a standard approach in terms of execution speed as the model complexity J increases. Although it was never required for DIII-D, the total execution time could be improved further by optimizing the computation of gradients of mutual inductances (which is beyond the scope of this Note).

The added dissipation rate $(1/2)\nu\dot{z}^2$ can be justified as a representation of otherwise unmodeled high-frequency magnetic damping effects. The damping effect exerted by the conductors on the rigid plasma is essentially a low pass filtered force, driven by $\dot{z}$. This damping is not correctly modeled at higher frequencies. It has been documented that in the tens of kilohertz range, for DIII-D, magnetic braking modeling of rotating plasma modes need to include Graphite tiles (these are not part of the axisymmetric standard model for vertical stability and shape control) [19]. At the same time, for the conductors that are included, skin effects increase the effective resistances, thus shorten the eddy time-scales and increase the bandwidth of the damping. Detailed modeling of this can

quickly become complex.

To be able to edit-out the oscillatory motion, while retaining a proper velocity state, without adding complexity to the model (such as adding short time scale passive elements) can be highly useful in e.g. fast nonlinear simulations, allowing larger integrator time-steps. Possible future applications of the fast growth-rate calculation methods reported in this note include gain-scheduled feedback control, and extensions to the more general cases including radial motion, and plasma current dynamics. There are also under-explored options to re-parametrize magneto-mechanical Lagrangians such as (1) to go beyond rigid models while still keeping dimensionality low.

Acknowledgement

This work was supported in part by the U.S. Department of Energy, Office of Science, Office of Fusion Energy Sciences, using the DIII-D National Fusion Facility, a DOE Office of Science user facility, under Award Nos. DE-FC02-04ER54698.

References

[1] S.C. Jardin and D.A. Larrabee. Feedback stabilization of rigid axisymmetric modes in tokamaks. *Nucl. Fusion*, 22(8):1095–1098, aug 1982.

[2] E.A. Lazarus, J.B. Lister, and G.H. Neilson. Control of the vertical instability in tokamaks. *Nuclear Fusion*, 30(1):111–141, jan 1990.

[3] A. Portone. The stability margin of elongated plasmas. *Nucl. Fusion*, 45:926–932, 2005.

[4] M.L. Walker and D.A. Humphreys. On feedback stabilization of the tokamak plasma vertical instability. *Automatica*, 45(3):665–674, 2009.

[5] N. N. Bao, Y. Huang, B. J. Xiao, Q. P. Yuan, H. D. Zhuang, Z. P. Luo, Y. H. Wang, and R. R. Zhang. A real-time disruption prediction tool for VDE on EAST. *IEEE Transactions on Plasma Science*, 48(3):715–720, 2020.

[6] Na-Na Bao, Yao Huang, Jayson Barr, Zheng-Ping Luo, Yue-Hang Wang, Shu-Liang Chen, Bing-Jia Xiao, and David Humphreys. Tests of the real-time vertical growth rate calculation on EAST. *Chinese Phys. B*, 29(6):065204, jun 2020.

[7] Jayson L Barr, Brian S Sammuli, Dave A Humphreys, K Erik J Olofsson, Xiaodi Du, Cristina Rea, Will P Wehner, Mark D Boyer, Nicholas W. Eidietis, Robert Granetz, A W Hyatt, Tong Liu, Nikolas Logan, Stefano Munaretto, E J Strait, and Zhirui Wang. Development and experimental qualification of novel disruption prevention techniques on DIII-D. *Nuclear Fusion*, 2021.

[8] B.S. Sammuli, J.L. Barr, and D.A. Humphreys. Avoidance of vertical displacement events in DIII-

D using a neural network growth rate estimator. *Fusion Engineering and Design*, 169:112492, 2021.

[9] D. A. Humphreys, T. A. Casper, N. Eidietis, M. Ferrara, D. A. Gates, I. H. Hutchinson, G. L. Jackson, E. Kolemen, J. A. Leuer, J. Lister, L. L. LoDestro, W. H. Meyer, L. D. Pearlstein, A. Portone, F. Sartori, M. L. Walker, A. S. Welander, and S. M. Wolfe. Experimental vertical stability studies for ITER performance and design guidance. *Nucl. Fusion*, 49:115003, 2009.

[10] R. Albanese, B. Carpentieri, M. Cavinato, S. Minucci, R. Palmaccio, A. Portone, G. Rubinacci, P. Testoni, S. Ventre, and F. Villone. Effects of asymmetric vertical disruptions on ITER components. *Fusion Engineering and Design*, 94:7–21, 2015.

[11] V.I. Arnold. *Mathematical Methods of Classical Mechanics*. Graduate Texts in Mahematics. Springer Verlag, 2nd edition, 1989.

[12] Gene H. Golub and Charles F. van Loan. *Matrix Computations*. JHU Press, 4th edition, 2013.

[13] Hanno Essén. From least action in electrodynamics to magnetomechanical energy—a review. *European Journal of Physics*, 30(3):515–539, mar 2009.

[14] D. Pfefferlé and A. Bhattacharjee. Algebraic motion of vertically displacing plasmas. *Physics of Plasmas*, 25(2):022516, 2018.

[15] Gene H. Golub. Some modified matrix eigenvalue problems. *SIAM Review*, 15(2):318–334, 1973.

[16] S. N. Bhattacharyya. Ideal magnetohydrodynamic stability in the presence of a resistive wall. *Physics of Plasmas*, 2(12):4381–4388, 1995.

[17] A. W. Hyatt, J. R. Ferron, D. A. Humphreys, F. R. Chamberlain, R. D. Johnson, B. G. Penaflor, D. A. Piglowski, J. T. Scoville, and M. L. Walker. Physics operations with the DIII-D plasma control system. Proc. 23rd IEEE/NPSS Symposium on Fusion Engineering, 2009.

[18] J. R. Ferron, M. L. Walker, L. L. Lao, H. E. St. John, D. A. Humphreys, and J. A. Leuer. Real time equilibrium reconstruction for tokamak discharge control. *Nucl. Fusion*, 38:1055, 1998.

[19] N C Logan, E J Strait, and H Reimerdes. Measurement of the electromagnetic torque in rotating DIII-D plasmas. *Plasma Phys. Control. Fusion*, 52(4):045013, mar 2010.